Chemical Science

Accepted Manuscript

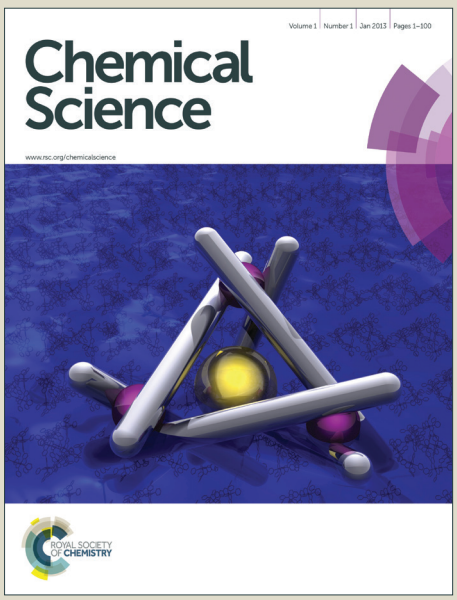

ROYAL SOCIETY OF CHEMISTRY

www.rsc.org/chemicalscience

Chemical Science

RSCPublishing

ARTICLE

Recent Advances of Ultrafast X-ray Spectroscopy in Chemical Sciences

v .,m,Cite this: DOI: 10.1039/x0xx00000x

L. X. Chen,[a,b] X. Zhang,[c] M. L. Shelby[b]

Received ooth January 2012,
Accepted ooth January 2012

DOI: 10.1039/x0xx00000x

www.rsc.org/

As an X-ray method for capturing transient structures of molecules during chemical reactions, X-ray transient absorption (XTA), or laser initiated time-resolved X-ray absorption spectroscopy has seen its capabilities greatly expanded in the past decade. XTA, which includes X-ray absorption near edge structure (XANES) and X-ray absorption fine structure (XAFS), has evolved beyond proof-of-concept studies and has been increasingly used to interrogate real chemical problems. Advances in ultrafast laser technology, pulsed X-ray sources in synchrotron facilities, as well as the frontier femtosecond X-ray pulses from X-ray free electron lasers open new opportunities to gain a new fundamental description of chemical sciences. This review reports historical and recent advances in XTA, particularly in its chemical applications, and is focused on 1) an overview of XTA capabilities in comparison to the related techniques of X-ray emission spectroscopy (XES) and resonant inelastic X-ray scattering (RIXS), 2) general chemical properties that can be investigated by the XTA method, 3) chemical systems studied by XTA investigations such as transition metal complexes, metalloproteins and hybrid systems, and 4) summary and perspectives.

Introduction

Ultrafast X-ray spectroscopy is defined by time resolution, X-ray photon energy and detection method. Based on the use of the term in a literature survey, the meaning of "*ultrafast*" in the X-ray regime in the past decade ranges from femtoseconds to tens of picoseconds and is limited by the pulse duration from sychrotron X-ray sources, free electron lasers, and table top ultrafast laser driven light sources. In comparison, only time resolution in the range of ~100 femtoseconds and less is now categorized as "ultrafast" in the optical regime. Historically, the term "ultrafast" has evolved with the technology and refers to the time resolution achievable with the technology in the forefront of dynamical science. "*X-ray*" here includes a wide range of electromagnetic radiation with energies ranging from tens of electron volts (eV) to hundreds of thousand eV, and is divided into "hard" and "soft" X-rays based on their energies. Hard X-rays typically have photons with an energy range from several keV to > 100 keV while the soft X-rays photon energies are those below this range. X-ray *spectroscopy* includes several spectroscopic techniques detecting signals after the X-ray photoexcitation of the materials, such as X-ray absorption near edge structure (XANES), X-ray emission spectroscopy (XES), resonant inelastic X-ray scattering (RIXS) and extended X-ray absorption fine structure (EXAFS). Descriptions for each of these techniques will be beyond the scope of this review. Hence, only brief descriptions will be given along with references for future reading. Instead, we focus on capabilities of these techniques in studying chemical systems and some recent advances in using these spectroscopic methods on the ultrafast time scale.

Our knowledge of chemical sciences has been closely associated with the molecular structural information available, which provides insight into reaction trajectories, energetic pathways, as well as dynamic structural evolution associated with these processes. Chemical phenomena take place on time scales that span many decades as shown in Figure 1. In order to capture how bulk reactions take place at the level of individual molecules, atoms, and electrons, molecular structural and electronic evolution through time must be synchronized. Otherwise, we can only detect equilibrium population changes as reactants become products in the bulk rather than molecular structures at each fundamental chemical event along the reaction trajectory. Advances in microscopy techniques combined with ultrafast laser spectroscopy now allow some reactions to be detected at the single molecule level, but a vast majority of the reactions are still being studied in molecular ensembles.

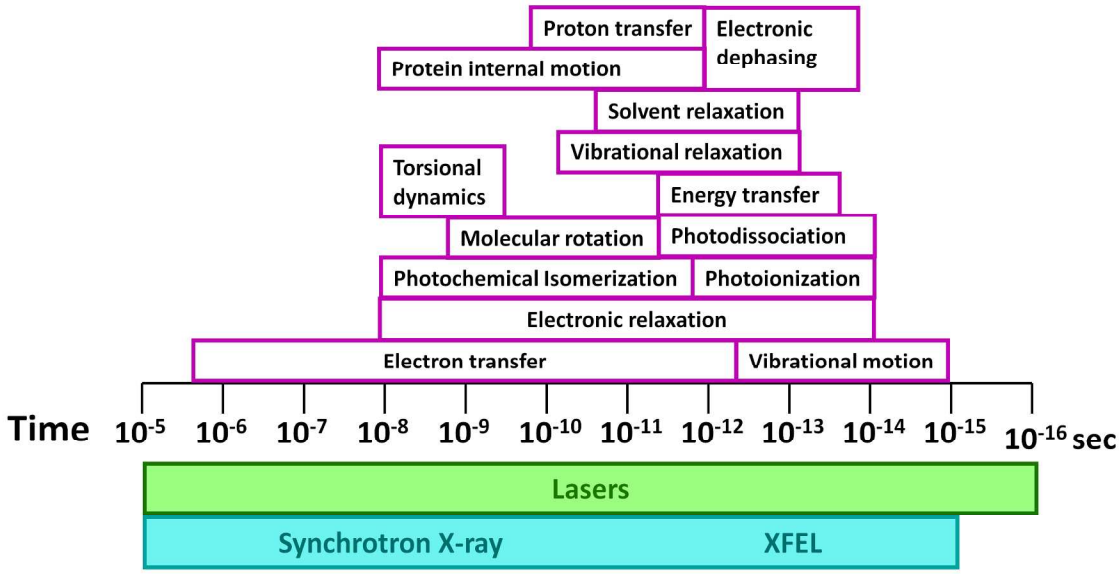

Figure 1. Time scales of some chemical processes and corresponding tools for studying them.

In order to synchronize molecular processes with the detection of molecular structure, energetics, and correlations between different reactive states, the "pump-probe" approach has been used in many ultrafast X-ray studies. This is inspired by the same approach used in optical spectroscopy for many years where an ultrafast external "pump" pulse is used to trigger a reaction in the sample. A second pulse, the "probe", follows to detect changes in the sample after the pump pulse. The most commonly used pump pulse is a laser pulse because its pulse duration can be as short as femtoseconds (1 fs = 10^{-15}s) (note: or even attoseconds, 1as = 10^{-18}s), compatible with many elemental chemical events such as vibrational motions in the molecules, which can be the first atomic movements leading to chemical reactions. Other "pump" sources with longer triggering durations, such as electric field changes, temperature/pressure jumps and mixing, can be used for studying slower processes, such as those induced by thermal effects. The probe pulse in optical transient absorption spectroscopies is the second laser pulse which detects the optical absorption/emission changes of the molecules after the photoexcitation, from which the optical signatures of the transient species can be detected. The probe used in ultrafast X-ray spectroscopy is an X-ray pulse that probes the X-ray absorption, emission and scattering signal changes after the laser pump pulse, each technique detecting the transient X-ray absorption spectra using different detection methods at a well-defined time delay from the pump pulse. As the spectra at different time delays from the pump pulse are obtained, one can extract intermediate state information as a function of time. The important feature in all "pump-probe" approaches is that the time resolution of the experiment is not determined by the detector response time, but the pulse duration of the pump and probe, whichever is longer, convoluted with the instrument response function (IRF), as long as the single pulse signals can be isolated from those of other pulses in time. The IRF caused by different nonlinear optical effects from the optics used in the setup is important for the femtosecond X-ray experiments as shown in the later section, but is unimportant in synchrotron X-ray experiments because the pulse duration of ~100 ps is much longer than the IRF broadening.

Ultrafast X-ray spectroscopic methods included in this review (Figure 2) can be divided into two categories, 1) XANES, XES and RIXS directly detect inner shell electronic transitions and describe complementary electronic transitions to the valence transitions obtained from optical spectroscopy, while nuclear geometry information can be deduced the electronic energy; levels of the occupied or vacant orbitals 2) EXAFS and RIXS detect resonant scatterings signal based on the interference of different photoelectron waves scattered by nearby atoms in the molecule, which can be transformed into an atomic radial distribution centered at the X-ray absorbing atom in the molecule, providing nuclear geometry information. Experimentally, XANES and EXAFS data are often collected together in ~1 keV energy range of the X-ray photon energy near a particular absorption edge. Frequently, "X-ray absorption spectroscopy" (XAS) is used to describe both XANES and EXAFS, which will be used in this review. Pioneered by Stern, Lytle and Sayers four decades ago,[1-3] and further developed in data analysis methods by Rehr and others,[4-7] XAS is now a commonly used method at synchrotron facilities. Because it is element specific and unrestricted to sample phase (solid, liquid, and gases), XAS is particularly suitable for studying species in dilute solution where many chemical reactions occur. As electronic transitions in other energy regimes (e.g., UV/visible), electronic transitions measured by XAS from an inner shell level (i.e., 1*s*, 2*s*, 2*p*, 3*d*,

etc.) to higher unoccupied orbitals and then to the continuum, measured are dipole mediated in the first order approximation. XAS transitions obey Fermi's Golden Rule, where the transition energy and the symmetry requirements must be fulfilled for a particular electronic transition, such as $1s \rightarrow 4p_z$, etc. The absorption profile $\mu(E)$ is hence proportional to $\sum|\langle f|\boldsymbol{e}\cdot\boldsymbol{r}|i\rangle|^2$, where $|i\rangle$, $|f\rangle$ are the initial state and final state, and $\boldsymbol{e}$ and $\boldsymbol{r}$ are the electromagnetic field vector and the transition dipole vector, respectively.

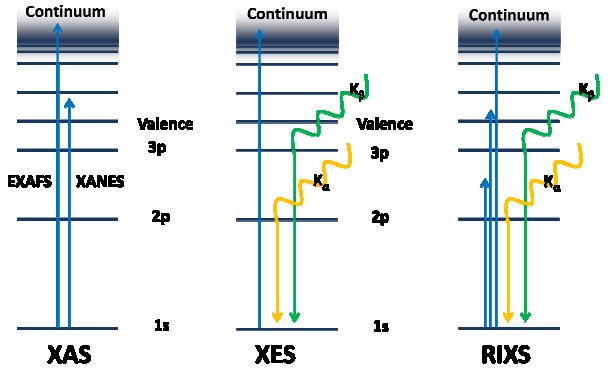

Figure 2. Comparison of the three X-ray spectroscopic methods in terms of electronic transitions.

The XANES spectrum covers -20 – 100 eV region relative to the absorption edge energy E_0, where transitions from the core level ($1s$, $2p$, etc.) to higher energy unoccupied levels are present. Some of the pre-edge transitions are dipole forbidden but quadrupole-allowed with weak intensities that, in some cases, can be used to identify the spin states and energies of unoccupied orbitals.[8] Some distinct and intense spectral features can appear in the middle of the transition edge for dipole allowed transitions, such as the $1s \rightarrow 4p_z$ transitions of first row transition metal complexes. Therefore, XANES spectra provide *information about empty orbitals* which the core electron can fill when excited.

The EXAFS region covers the energy range 50 eV or higher than E_0 at which the inner shell electron is completely ejected to the continuum. While the same $\mu(E)$ is still proportional to $\sum|\langle f|\boldsymbol{e}\cdot\boldsymbol{r}|i\rangle|^2$, the final state is modulated by the scattering by the neighbouring atoms and the EXAFS signals occur from the interference of the outgoing photoelectron wave originating at the central X-ray absorbing atom and the back scattered photoelectron wave from neighbouring atoms, which can be described by the equation below:

$$\chi(k) \propto \sum_j N_j F_j(k) e^{-2\sigma^2 k^2} e^{-\frac{2r_j}{\lambda_j(k)}} \frac{\sin[2kr_j + \delta_{ij}(k)]}{kr_j^2} \quad (1)$$

where j is the index for the neighboring atom shells around the X-ray absorbing atom, $F(k)$ is back-scattering amplitude, N, coordination number, r, average distance, σ, Debye-Waller factor, λ, the electron mean free path, and δ is the phase shift of the photoelectron wave. k is photoelectron wavevector, $k = [2m(E-E_0)/\hbar^2]^{1/2}$, where m is the electron mass and E_0 the threshold energy for the transition edge. In principle, XAS (XANES and EXAFS) can be formulated via multiple scattering theory as shown in the literature.[4-7] EXAFS spectra are used to obtain atomic distances in the form of a radial distribution function centered at the X-ray absorbing atom.[9, 10] Because the scattering paths are sensitive to both inter-atomic distances and the orientation of the scattering wavevectors, XAS spectra can be used to extract atom-to-atom distances with high precision as well as angles between different bonds for distant coordination shells.[9] Experimentally, XAS signals can be detected using transmission or fluorescence mode which is from the total X-ray fluorescence arisen from outer shell electrons refilling the hole in the inner shell (Figure 2) and hence the X-ray fluorescence intensity is proportional to the X-ray photons absorbed by the sample. The X-ray fluorescence detection is a more sensitive method than transmission for dilute samples because the majority of elastic scattering background signals can be removed by low pass filters leaving only the X-ray fluorescence signals to be collected.

XES detects X-rays emitted from the sample with an instrumental energy bandwidth comparable to the line width of the corresponding core-hole lifetime broadening.[11, 12] XES includes high energy resolution X-ray fluorescence spectroscopy (e.g. K_β spectroscopy), resonant X-ray emission spectroscopy (RXES) and resonant inelastic X-ray scattering (RIXS). After an inner shell excitation (e.g., $1s \rightarrow 4p_z$, transition), a hole created in the inner shell will be immediately (in 10^{-15} s or fs = femtosecond) filled by an electron from a higher energy orbital, producing an emission line. The main difference between XES and XAS with X-ray fluorescence detection is the spectral resolution of the emission. The former resolves different emission lines shown in Figure 2 and hence extracts elemental/environmental specific electronic structure according to emission energies from the occupied orbitals to the core hole. The latter detects the total emission signals proportional to the inner shell population that is related to the transition from the inner shell orbital to an unoccupied orbital. Therefore, an XAS spectrum reflects the unoccupied density of electronic states while an emission spectrum is related to the density of occupied states. XES detects emission lines with sufficiently high energy resolution to resolve the energy modulation of the absorbing atom orbitals and their occupation due to electronic structural changes, such as change in oxidation state, spin state and electronic coupling with the environment. These energy resolved emission lines can be obtained by the X-ray excitation with photon energies well above the transition edge energy of the element of interest. Therefore, they are not limited to have photons at exact edge energies of the X-ray absorbing atoms as in XANES. The energy and intensity of the emission lines are determined by Fermi's Golden rule which considers not only the density of the occupied orbitals higher in energy than the core hole, but also selection rules based on the symmetry of the matrix

element of a dipole mediated transition, $\sum|\langle f|\boldsymbol{e}_x\cdot\boldsymbol{r}_x|i\rangle|^2\,\delta(E)$. The XES detection system can provide energy resolution of 0.6 - 1 eV while most of X-ray fluorescence detectors used in XAS have either no means of energy discrimination or at most a few hundred eV resolution if a solid state semiconductor detector is used. A detailed description of XES can be found in two reviews by Glatzel and Bergmann[11, 12] and references therein. RIXS is a special case of XES with the X-ray photon excitation resonant at particular inner shell to valence orbital transition and the emission spectrum is collected as a function of the X-ray excitation photon energy.[11, 12] A full set of RIXS data is a three-dimensional intensity map, with the X-ray photon excitation energy on x-axis and X-ray emission photon energy on y-axis. It is a photon-in (excitation) and photon-out (emission) technique with most applications so far in solid state physics and materials sciences. RIXS can be viewed as an analog of excitation wavelength dependence fluorescence spectra (or excitation spectra) in the optical regime. However, the interpretation of RIXS results can be complicated and is a currently very active research area.

Thus, XAS (XANES and EXAFS), XES and RIXS are complementary methods; each has its advantages and limitations. In this review, we will focus on the most commonly used ultrafast XAS method in detail and suggest readers to seek details of ultrafast XES and RIXS methods through recent literature.[11-19]

Chemical Problems Studied by Ultrafast X-ray Spectroscopies

Ultrafast X-ray transient absorption (XTA) spectroscopy using the *pulsed nature* of the synchrotron X-ray source with the "pump-probe" approach started about 15 years ago when intense X-ray pulses with 30 – 100 ps duration became available from third generation synchrotron sources.[20, 21] In the past decade, XTA has been applied to various systems in chemistry, biology, materials sciences and physics as described by several reviews.[22-26] Now fourth generation femtosecond X-ray sources, namely X-ray free electron lasers, are operating in different facilities around the world, and are used for taking "snapshots" of molecular processes using the "pump-probe" approach. It is therefore useful to highlight unique and complementary information provided by ultrafast X-ray spectroscopy to the chemistry community as described below.

Metal center oxidation state Many metal centers in transition metal complexes, proteins, nanoparticles and solid films participate in reactions in which the charge density on the metal centers change. Metal centered redox processes are common in catalytic reactions. In order to obtain detailed reaction mechanisms, one needs to know transient metal center oxidation states at different stages of the reaction of interest. Although metal oxidation state information can be obtained by X-ray photoelectron spectroscopy (XPS) in the soft X-ray or VUV/HUV region, the requirement for ultrahigh vacuum makes it difficult in the past to study metal containing molecules in the relevant chemical environment such as the solution phase. Recent progress has been made in XPS to study solution samples under the ambient pressure, which broadens its application significantly in the future.[27-30] Transient metal center oxidation state information can also be obtained via other spectroscopic methods, such as time-resolved vibrational spectroscopy where the metal oxidation change is reflected in the ligand vibrational frequency shifts, such as in the C=O or metal-ligand bond stretching frequency.[31-37] Also, it can be indirectly obtained via transient optical absorption where the distinct features associated with the metal oxidation state can be obtained.[38-42] Sometimes, these methods can yield ambiguous results due to the signal overlap of different species, the relatively low oscillator strengths for some metal centered transitions, or simply because the material can be optically opaque. X-ray transient spectroscopies provide a different set of transitions from the inner shell elemental orbitals to valence orbitals. The transition edge energy is directly related to the photoelectron binding energy which depends on the charge of the metal center. The higher the effective nuclear charge, the higher energy X-ray photon is needed in order to eject the core electron to the continuum. X-ray transient spectroscopies can also interrogate materials without perfect optical quality, such as powders, soots or suspensions/emulsions, which provides a huge advantage for studying catalytic reactions. As shown in Figure 3, comparing the K-edge XANES spectra of a copper (I) diimine complex in the ground state, the metal-to-ligand-

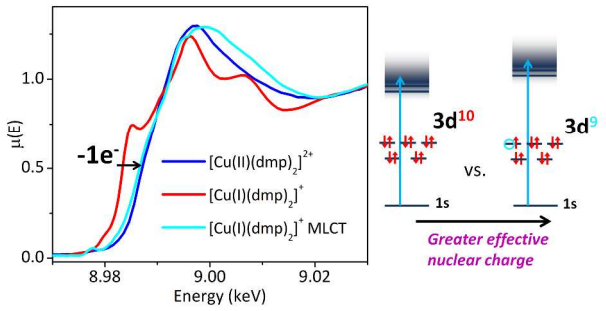

Figure 3. Left: Cu(I)/Cu(II) XANES spectra (remeasured recently) to demonstrate the features associated with the copper oxidation state change; Right: the energy levels, orbital vacancies and Fermi Golden Rule determine transition probability. The 1s →3d transition is quatrupole-allowed and only $3d^9$ allows one transition whereas $3d^{10}$ will not allow any transition in the pre-edge region.

charge-transfer (MLCT) state and its copper (II) counterpart in the ground state provided evidence for the identity of the MLCT state as copper (II) because the transition edge energy is shifted higher to coincide with that of the copper (II) species. The pre-edge feature at 8.978 keV suggested the electron vacancy in one of the 3d orbitals to enable the 1*s* to 3*d* transition through quadrupole interactions.

Metal centered electron configuration and orbital energies Relative energies of the reactants and intermediate states frequently determine the reaction pathway.[43] In many electron

or energy transfer reactions involving transition metal centers, the relative energies of the orbital that will accept or donate the electron and the energy of the donating or accepting surroundings is the key for determining the direction and rate of reaction.[44-49] Although high energy resolution gas phase spectroscopy or XPS in the vacuum can provide important references for the energy levels of transient states involved in chemical reactions, these energy levels in solution could change drastically due to the structural change of the solute as well as solute-solvent interactions.[44-49] By having a series of transition energies that are metal dependent, one can selectively probe the inner shell to high energy level transition energies associated only with the metal center, and hence obtain electronic structural information associated with metal centered orbitals. Characterization of these metal centered orbitals is not easily accomplished by transient absorption/emission spectroscopy and frequently relies on advanced quantum mechanical calculations. As shown in Figure 4, the pre-edge region of the nickel K-edge XANES spectra revealed distinct features originating from 1*s* to 3*d* transitions. The ground state Ni(II)

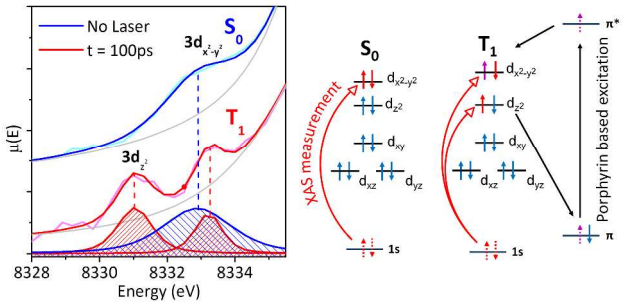

Figure 4. Left: NiTMP pre-edge spectra (redrawn from the data in Reference 51), and right: the molecular orbital energy levels and electronic configurations for the ground and thermalized excited states as well as the possible 1s → 3d transition

has a square-planar $3d^8$ electronic configuration, corresponding to vacancies at the highest energy $3d_{x2-y2}$ molecular orbital, resulting in only one transition from 1s to $3d_{x2-y2}$ molecular orbitals.[50, 51] In contrast, the excited state Ni(II) porphyrin showed two pre-edge peaks, corresponding to transitions from 1s to $3d_{x2-y2}$ and 1s to $3d_{z2}$ transitions, respectively, revealing the electronic configuration at the excited state as two singly occupied 3*d* orbitals with their transition energy separated by over 2 eV.[50, 51] XANES, XES and RIXS can all provide the electronic configuration for systems in solids, gas and solution, providing complementary information on electronic structures obtained from other techniques. XES and RIXS can even resolve the transition energies corresponding to different spin states, which has been extensively applied to resolve the spin crossover dynamics of Fe(II) complexes.[17, 19, 52-56]

Transient coordination geometry of the metal center during chemical reactions Many chemical reactions require changes in metal-ligand coordination geometry, such as small molecules binding and releasing from metal centers in catalysts and enzymes. Also, some metal complexes could have strong interactions between solvent molecules and the metal center via solvation or direct ligation.[50] A coordination geometry change is usually accompanied by an electronic structural change and vice versa, for example as in changes in d orbital occupation due to the electron transfer or spin state changes triggered by ligand binding or releasing.[57-66] Hence, the coordination geometry of the metal center can be used to modulate energy levels of metal centers, and electronic transitions observed through XANES, XES and RIXS can be sensitive to the coordination geometry. Meanwhile, EXAFS spectra provide accompanying distance and coordination number changes between the metal and ligand atoms. These capabilities have been shown via extensive steady-state as well as pump-probe measurements. Figure 5 shows one example of using a characteristic $1s \rightarrow 4p_z$ transition feature to monitor photo-induced ligation process of nickel tetramesitylporphyrin (NiTMP) in toluene/pyridine as a function of the pump-probe delay time, revealing the time required to stabilize the liganted species is around 600 – 800 ps.[50]

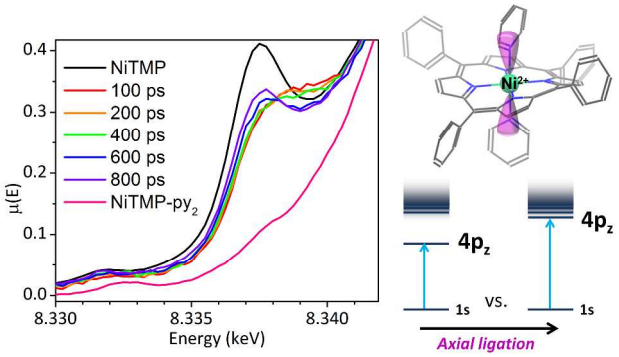

Figure 5. Left: the NiTMP $1s \rightarrow 4p_z$ transition as photo-induced ligation takes place as a function of the pump-probe delay time indicated by the legend (redrawn from the published data in Reference 50), and right: the $1s \rightarrow 4p_z$ transition energy increases as a function of the ligation state of Ni(II), as seen by a sharp feature at 8.3375 keV for the distorted square planar geometry shifted to a higher energy near the whiteline peak for the double axial ligated species, resulting in the disappearance of the sharp edge feature.

Method Development of Hard X-ray Transient Absorption Spectroscopy

In this section, we choose to focus on hard X-ray absorption spectroscopy within our expertise. For spectroscopy in the soft X-ray regime (i.e., <5 keV)[67-70] and XES/RIXS, we recommend several recent reviews on these topics.[18, 71]

Time resolution In general, the time resolution for the transient structural measurements using the pump-probe approach is determined largely by the pulse durations of the laser pump and X-ray probe, whichever is longer, convoluted with the instrument response function (IRF). The IRF needs to be considered in data fitting convoluted with the signal when the pulse duration is comparable with the time duration of the IRF, as seen in ultrafast optical spectroscopy and femtosecond

X-ray experiments. Because synchrotron X-ray pulses are much longer than the duration of the IRF due to optical components in the setup, it is largely neglected in most of the XTA data analyses in synchrotron based measurements with the X-ray pulse duration of ~80 ps. Shorter X-ray pulse durations from synchrotron sources have been achieved with a "slicing source" from synchrotron facilities where a strong femtosecond laser pulse interacts with a 100-ps long electron bunch to diffract a very small portion of the electron bunch, generating ~100 fs X-ray pulses.[72] Such short X-ray pulses have enabled a few spectroscopic measurements with very good time resolution, but which could take up to two weeks of beamtime to collect one XANES spectrum with limited number of data points[73] because the pulse slicing also lowered X-ray photon flux in each probe pulse by approximately three orders of magnitude than the original standard synchrotron pulse. The most drastic improvement of the time resolution is achieved at the fourth generation X-ray sources, the X-ray free electron lasers (XFELs), such as the Linac Coherent Light Source (LCLS), which will be described later.

Data quality in X-ray absorption spectroscopy The data quality of ultrafast X-ray spectroscopy is strongly related to the photon flux from the X-ray source to be used as probe pulses. The data quality requirements for extracting desirable information are method-dependent. For XES and RIXS, please refer to the reviews in recent years.[12, 18, 74-76] For the X-ray absorption spectroscopy, especially EXAFS, using either transmission or fluorescence detection, one can use the total signal amplitudes (or the edge jump) and the amplitude of the oscillation (EXAFS signals) to estimate the required signal to noise to enable correct data acquisition time.[22-24, 77] In the early stages of XTA development at the Advanced Photon Source (APS), the most commonly used laser pump repetition rate was 1kHz, which used only one X-ray pulse in every 6500 pulses in the X-ray pulse train to derive the shortest time delayed signal, resulting in an extremely low throughput. Frequently, each EXAFS spectrum with a ~500 eV spectral scan range took over 40 hours to acquire with limited data quality. Advances in accelerator science and technology drastically improved the X-ray photon flux and enabled beamlines with novel undulator device configurations, such as dual in-line undulators, which significantly improved photon flux by an order of magnitude. Synchrotron sources, such as the APS, can provide an average monochronnatic photon flux of $>5 \times 10^{12}$/sec on the sample, at some beamlines at a repetition rate of 6.5MHz, or $>10^6$ photons/pulse. This is equivalent to $>10^9$/sec for the average probe photon flux in pump-probe experiments running at 1kHz repetition rate. The improved stability of the X-ray beam and the sample delivery system also contribute to the improved data quality. A key improvement for the data quality for dilute samples with ~ 1 mM concentration of the absorbing atom comes from the novel data acquisition method with in-situ curve fitting of the pulsed X-ray fluorescence signals by Jennings at the APS (unpublished work). In this approach, a weak signal can appear as a noisy pulse with complicated pulse shape due to electronic noise in the detector or environmental effects. The conventional peak-height or integrated peak area detection could result in very inconsistent data with a high level of noise, or may simply make the weak signal undetectable. With the pulse fitting, or "shaping", implemented, background and the DC off-set are fit to functions before the pulse shape integration step to yield the signal intensity, drastically improving the data quality and filtering out high frequency noise as well as any artifact due to an irregular pulse shape. Therefore, much higher quality EXAFS for a solution with a few mM can be obtained within a few hours as shown in Figure 6. Combined with the in-situ curve fitting data acquisition routine is the capability to capture signals from the entire pulse

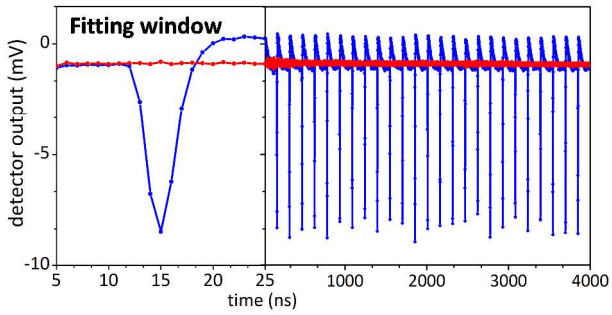

Figure 6. Illustration of in-situ data fitting. Left: fitting of a single pulse with 1 ns interval. Right: the signal from the detector from one revolution of the storage ring with 24 pulses at the APS. The blue is the signal, and the red is the dark background.

train between two pump laser pulses. At the APS, the most commonly used timing mode is "24-bunch mode" with a time interval of 153 ns between the X-ray pulses. Hence, it is now feasible to map out the chemical trajectory of a system following excitation with first the X-ray pulse set at a specific delay time with respect to the pump laser pulse, and then other pulses following at time delays separated by 153 ns. Such a capability is extremely important for some slow reactions, where multiple time points can be taken from a single pulse train without needing to separately collect XAS at those delays, such as those processes in metalloproteins. All these improvements significantly shortened the data acquisition time and have made X-ray transient absorption spectroscopy a much more widely used technique than a decade ago.

A recent important development that contributes to significant improvement of the data quality of XTA is the application of high repetition rate pump lasers that potentially could increase the pump-probe cycle as high as the X-ray repetition rate, 6.5MHz at the APS, while still offering sufficient pulse energy for the pump.[78, 79] Caution needs to be taken in considering the requirements for sample jet flow rates, recovery time as well as stability of the solute/solvent under high power laser illumination. Depending on the specific conditions for a particular chemical system, the proper repetition rate can be chosen. For example, the recovery of many transition metal complex excited states can be in the range from multiple

hundreds of nanoseconds to microseconds, which will not recover back to the ground state by the time the second X-ray appears 153 ns later as in the APS.

X-ray absorption spectroscopy, such as XANES, at femtosecond X-ray sources has been recently achieved as shown in the first such example from the LCLS on the spin crossover iron complexes.[79] The detailed description can be found in the later section of this review.

Sample selection and experimental platform As the X-ray facilities improve significantly, hard X-ray spectroscopic measurements can be carried out on many forms of sample, powder, solution, liquid, amorphous, gas phase or single crystal. For laser pump, X-ray probe measurements, the sample does not have to have a high optical quality as required for optical transient absorption spectroscopy. While samples are often run in solution phase for X-ray transient absorption (XTA) spectroscopy, liquid/solid suspensions and liquid/liquid emulsions can all be studied by this method because all these can be recirculated by a liquid pump and liquid jet system to minimize the local heating and radiation damage by the laser or X-ray photons. Currently, the volume required for the sample circulation can be as small as ~20 ml. It is clear that more sample platforms are needed to accommodate the variety of chemical systems. Recently, low temperature XTA experiments in cryostats were implemented with developing protocols for liquid or solid samples. As many solid inorganic materials are found to play important roles in chemical reactions, such as catalysis and solar cell/solar fuel generation, XTA experiments have also been conducted by rastering solid film samples during aquisition. Other new sample environments to be implemented in XTA measurements include in-situ electrochemical cells with external voltages.

Combined studies using optical and X-ray transient absorption spectroscopies and scattering Most of the pump-probe X-ray spectroscopy measurements are "photon hungry" experiments. Therefore, extracting the most structural information per incident X-ray photon is challenging and beneficial for optimization of the photon usage. Recent experiments combining XAS, XES and RIXS at the synchrotron and XFEL have been successful in taking advantage of the orthogonality of detection gemoteries required by different X-ray spectroscopic methods, summarized in Figure 7 with our depiction.[8, 17, 74, 75, 80]

In this set of the experiments, three techniques were simultaneously used, XAS, XES and X-ray scattering in solution samples. The first two methods provide information about the electronic structures of the Fe(II) center in $[Fe(II)(bpy)_3]^{+2}$ and the third method will obtain nuclear structures of the complex as well as the surrounding solvent molecules in the ground and the excited states. XANES and EXAFS can provide the same information with more precise local structure of the neighboring shells, but the a relatively large energy range of more than 500 eV demands better optical and mechanical components at the beamline, the energy resolution is lower, and the technique is less sensitive to distant

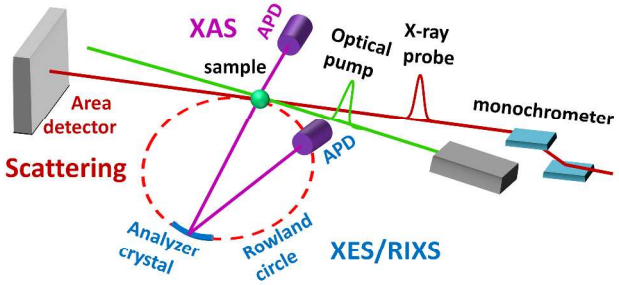

Figure 7. Illustration of combined XAS, XES and RIXS measurements at a synchrotron source.

atoms, such as solvent molecules and the overall molecular shape. Nevertheless, the detection for XANES and EXAFS signals in low concentration samples is preferably the X-ray fluorescence method, which often requires only PMTs or ADPs coupled with the elastic signal blocking filters and slits at 90° to the incoming beam, which is much simpler to setup and more portable than those for XES or RIXS, which requires either multiple bent crystals for each transition edge or elaborate control mechanical systems for crystal bending in order to discriminate against the elastic scattering signals and achieve much higher energy resolution as shown in the reviews by Bergmann and Glatzel.[12] One can choose a method that addresses the scientific questions of interest.

Examples of recent advances in ultrafast X-ray spectroscopy

Excited state dynamics of transition metal complexes (TMCs) Transition metal complexes (TMCs) have important applications in many areas, such as solar energy conversion, catalysis, photonics and metalloprotein enzymatic function. Because their reactivity is often closely associated with the local electronic and nuclear structure surrounding the metal center, X-ray absorption spectroscopy is an important tool for determining structural origins of chemical properties. Metalloporphyrins and transition metal polypyriduyl complexes were chosen as the first proof of concept systems to prove the feasibility of XTA.[20, 21] More recently, XTA methods have been applied to a variety of different transition metal complexes related to solar energy conversion, spintronics and catalysis.[25, 52, 60, 73, 79, 81-96] XTA measurements are not limited to samples with high optical quality and can be used on emulsions/suspensions and to extract transient states that are optically dark.[50, 97]

Two common photoinduced transitions among TMCs are metal-to-ligand-charge-transfer (MLCT) or ligand-to-metal-charge-transfer (LMCT) transitions that shift electron density between the metal centers and ligating groups, and are often accompanied by nuclear geometry changes in response to the electron density rearrangement.[95, 98-101] However, it is not often clear what exactly happens to the metal centers in TMCs in terms of their oxidation state and detailed coordination geometry changes, which hinders our understanding and rational design of TMCs for converting light energy to electrons or redox equivalents. In particular, many catalytic reactions, such as water splitting, require two or more

electrons while light absorption from sunlight consists of successive single photon absorption events as opposed to multi-photon processes. To determine photocatalytic pathways, optical spectroscopy alone cannot extract metal center structural information, because 1) the optical signatures of the functional metal centers in condensed phases are often overlaid with and weaker than the $\pi \rightarrow \pi^*$ transitions of aromatic ligands; 2) metal-centered excited states may be optically dark or optical absorption indistinguishable; and 3) most time-resolved vibrational spectroscopy studies of transition metal complexes are focused on characteristic frequencies of certain functional groups (e.g. carboxyl groups, etc.)

Recently, excited state structures of a nickel porphyrin and its ligation with pyridine not only demonstrated current XTA capabilities in synchrotron sources, but also provided new structural dynamics information that we were unaware of without XTA results.[50, 51] It has been recognized that ground state Ni(II) porphyrins are non-planar and convert between several possible conformers coexisting in solution at room temperature,[102, 103] but it was unclear how such non-planar distortions influence the 3d orbital energies. An interesting observation in the XANES spectra of distorted square planar nickeltetramesitylporphyrin (NiTMP) at the Ni K-edge came from comparing the widths of the pre-edge features of the ground and excited state NiTMP. The former has an electronic configuration of $3d^8$ and the highest two molecular orbitals with occupations $(3d_{z2})^2(3d_{x2-y2})^0$. Hence, the ground state has one $1s \rightarrow 3d_{x2-y2}$ pre-edge transition peak of > 2 eV fwhm. In comparison, at nominally 100 ps delay the relaxed excited state with ~200 ps lifetime, has two transitions, $1s \rightarrow 3d_{x2-y2}$ and $1s \rightarrow 3d_{z2}$, which arise from an electronic configuration $(3d_{z2})^1(3d_{x2-y2})^1$ with ~0.8 - 0.9 eV fwhm respectively (Figure 4), assumed to be the spectral resolution limit imposed by monochromator energy resolution and core-hole lifetime broadening.[50, 51] The wider ground state pre-edge peak reflects a rather large $3d$ orbital energy distribution in a solution environment with coexisting and inter-convertible non-planar conformations, while the total molecular energies, including the surrounding solvent molecules among conformers, can still be within kT (k, Boltzmann constant and T, temperature).[50] This assessment has been verified via DFT calculated $3d$ orbital energy levels of a series of conformers[50] inferred by previous Raman studies.[102, 103] When the $3d$ orbital energies vary as much as 1 – 2 eV among the conformers, the $3d_{z2}$ and $3d_{x2-y2}$ orbitals could transiently become isoenergetic in certain conformers, enabling electrons to hop from one $3d$ orbital to another, e.g. from $3d_{z2}$ to $3d_{x2-y2}$. A 0.09 – 0.1 Å elongation of the Ni-N bond distance in the T_1 state (Figure 3B) revealed by our studies suggested an enlarged effective Ni(II) radius as one electron was added to the anti-bonding $3d_{x2-y2}$ orbital while the other electron is removed from the lower energy $3d_{z2}$ orbital.[50, 51] A larger Ni(II) radius in the relaxed excited state makes a better fit between Ni(II) and the porphyrin cavity, and hence results in much more planar porphyrin conformation and less structural divergence as seen by the narrower double pre-edge peaks (Figure 3A). Only when $3d_{z2}$ orbital has a vacancy in the excited state can it accommodate lone pair electrons from the N atom in pyridine ligands, and hence acquires axial ligands evidenced by the reduced intensity in the $1s \rightarrow 4p_z$ transition peak (Figure 3), as the peak position is moved to a higher energy.[104]

In the presence of the solvent molecules that are capable of ligation in the ground and excited states, the excited state lifetime was prolonged to allow the additional ligation in 600 – 800 ps after photoexcitation (compared to ~200 ps in the absence of pyridine).[104, 105] These studies enabled the direct observation of the excited state ligand and metal binding interactions on the atomic and electronic scales. They also established a unified ligation mechanism for the ground and excited states with the common prerequisite of the $3d_{z2}$ vacancy, created either via electron hopping from transiently degenerate $3d_{z2}$ to $3d_{x2-y2}$ in the ground state, or via photoexcitation.

Canton et al., recently carried out XTA measurements at the Co K-edge on a photoinduced electron transfer reaction in a covalently linked electron donor (D), the MLCT state of a Ru(II) bipyridal complex, to an electron acceptor (A), a Co(III) bipyridal complex. The XAS collectionwas combined with X-ray emission spectroscopy (XES) studies and quantum mechanical calculations.[97] They observed the reduction of Co(III) to Co(II) as the result of electron transfer and a spin flip accompanied by an average Co-N bond elongation of 0.20 ± 0.03 Å.[97] The data quality was sufficiently high so that the detailed structural information can be extracted with confidence. Both the XTA spectra of the above NiTMP example and this covalently linked D-A complex show very informative pre-

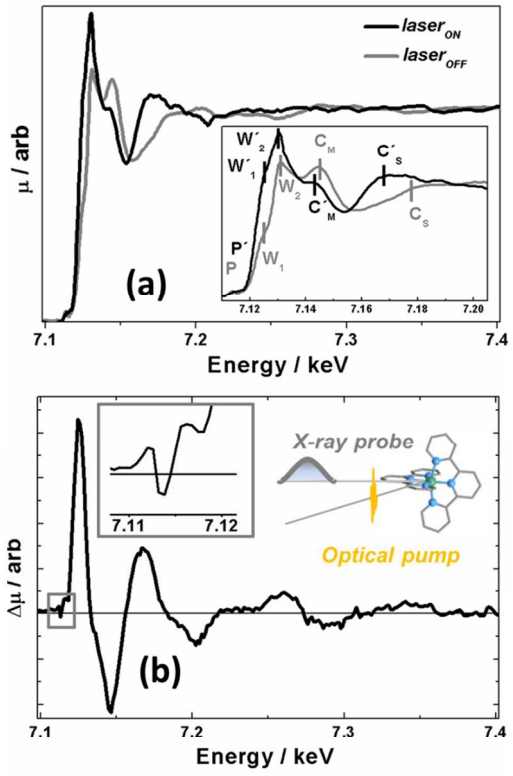

Figure 8. The light induced spin crossover in Fe(II)bis-terpyridal complex by Canton et al.(Ref. 80). (a) Normalized X-ray absorption (XA) spectrum μ without (gray) and with (black) laser illumination for $[Fe(terpy)_2]^{2+}$ in MeCN, at a pump−probe time delay of 200 ps. The inset zooms on the near edge region. (b) Difference XA (DXA) spectrum Δμ. The inset zooms on the pre-edge region. (Permission from *J. Phys. Chem. C*, American Chemical Society).

edge features which clearly identified the relevant spin states or orbital occupations on the time scale from 80 ps, which current electron paramagnetic resonance (EPR) methods cannot obtain. Similar XTA measurements can be applied to many TMC systems that are currently used in catalysis and solar fuel/electricity generation.

One type of system that has been extensively investigated by XTA is light induced spin crossover processes in iron(II) complexes[106-108],led by the XTA investigation by Kahlil et al.[109] and followed by several extensive investigations by different groups.[84, 110-113] The iron(II) spin crossover complexes are a very good platform for studying closely correlated nuclear geometry and electronic structure in transition metal complex systems because both nuclear and electronic structural change yield distinct and trackable XANES and XAFS features to enable both experimental and theoretical investigations.[17, 52-56, 73, 79, 84, 90, 93, 107, 108, 114] A typical light induced iron(II) electronic spin state crossover XTA spectra in a recent work is shown in Figure 7, where both XANES and difference XAFS spectra as well as the pre-edge features clearly showed electronic spin transition from $3d^6$, s=0 to s=2, with a typical expansion of the Fe-N bond by 0.2Å. However, with high signal to noise ratio, the differences of the Fe-N bond lengths in Fe-terpyridyl ligand, one central Fe-N distance vs. two distal Fe-N distances in each ter—pyridyl ligand can be extracted. Such progress is important for many chemical systems with subtle variations in structure as a result of photoexcitation or other sources of perturbation.

Cu(I) diimine systems have been increasingly studied via the XTA method in the past decade focusing on structural factors including conformation and solvent-solution interactions which can strongly influence the MLCT state properties, such as lifetimes and fluorescence yields.[87, 115-117] These complexes have been applied to solar energy conversion, catalysis as well as photonic materials. The Cu(I) to Cu(II) conversion due to the photoexcitation also generates distinct features at the copper K-edge XAS spectra which can be used to monitor the reaction trajectories in photochemical reactions as shown in a recent review as well as references therein.[118]

The above examples are from the first-row transition metal complexes that have relatively narrow transition band widths compared to those of higher row transition metals with homogeneously broadened pre-edge and edge features due to the shorter core-hole state lifetimes. However, there are a number of the second and third row transition metal complexes studied by the XTA method, such as ruthenium,[21, 97, 113, 115, 119-122] iridium,[123] rhenium,[83] platinum[13, 117] and tungsten[124] complexes. XTA has also been used on multiple-metal-center complexes, such as $Ru_3(CO)_{12}$[60] and $Ru_2(Cp)_2(CO)_4$[119] (where CO is carbonmonooxide and Cp, cyclopentadiene), these complexes undergo photoinduced isomerization, sometimes irreversible, while converting light energy to heat or catalyzing chemical reactions. Some of these complexes were extensively studied by time-resolved vibrational spectroscopy focused on the C≡O stretching signal.[60] While the C≡O stretching frequency can be sensitive signatures to the local structure, they provide indirect information on transient coordination geometry and oxidation state of the metal center. XTA can offer complementary information to the time-resolved vibrational spectroscopy to enable us to capture snapshots of these transient species in a novel way.

Intermediate States of Metalloprotein Ligand Dissociation

As XTA matures as a technique, it has found application in more and more technically challenging systems, including metalloproteins. Though these systems have a host of experimental challenges including scarcity of sample, difficulty of producing highly concentrated solutions, and sensitivity to damage by both laser and X-ray, years of small molecule studies have informed XTA signal to noise optimization and control of the sample environment.[125, 126 20, 22, 26, 50, 51, 59] For enzymes with a metal centered active site, catalysis often involves changes in oxidation state, coordination, and other geometric or electronic changes at the metal. Because of their very large molecular weights and the chemical diversity of potential protein-bound cofactors, the elemental specificity of XES/RIXS/XAS is particularly useful to pick out these changes compared to optical or scattering techniques. Transient dispersive XES is an emerging technique to address questions of metal center oxidation state, elemental identity, and, indirectly, structure at protein active sites. Dispersive XES is finding especial utility for sensitive systems such as photosystem II at free electron lasers where the high number of photons/pulse allows maximum signal collection before the sample ultimately undergoes radiation damage.[13-15]

While time resolved SAXS, crystallography, and dispersive XES have been increasingly used to study protein systems, XTA demands the additional necessity of scanning the X-ray probe energy and so far fairly few XTA studies of biological systems exist. If the X-ray absorption spectra of starting materials and products are well defined, one can use the transient X-ray absorption at a single energy as a kinetic trace where this is not available from conventional TA. For example, this approach was taken in the observation of changes in the edge position, and thus the oxidation, of the Mn cluster of photosystem II on excitation observed by Dau et al.[127, 128] However, if one is interested in structural characterization of reaction intermediates and transient states, full XANES or EXAFS spectra are necessary to fully access the power of XAS to describe chemical systems.

To date biological XTA studies have largely investigated the recombination of iron heme biding diatomics in the oxygen carrier myoglobin following optically-induced photolysis. Diatomic-binding hemoproteins in the globin family have been increasingly demonstrated to have a complex set of physiological functions that extend beyond O_2 transport. Sensing of endogenously produced CO and NO has been implicated in a number of signaling pathways, and in binding these signaling molecules, as in the binding of O_2 by Hb, an allosteric conformational change in tertiary structure is triggered by the movement of Fe into the porphyrin plane. For this process, the basic nature of diatomic ligation and how it is mediated by factors imposed on the heme by the protein matrix is of fundamental importance, as demonstrated by the variation

of diatomic binding affinities between globins and as a result of changes in the allosteric state exemplified by the R to T transition Hb. In the case of CO dissociation from Mb, the dynamics of both structural and electronic changes at the heme during ligand dissociation and association promise to reveal the complex relationship between spatial and temporal physical properties and function.

Three decades ago, pioneering work by Mills[129] tracked changes in the Fe K-edge position due to the loss of the electron withdrawing effect of the backbonding CO ligand following the photolysis of CO with a time resolution of 300µs. Later work by Wang[124] improved this time resolution to 100µs and improvements in the laser repetition rate lead to much higher signal to noise. This enabled the observation of the low spin to high spin transition of the d electrons on photolysis by analysis of the 1s to 3d transitions.

In the past a few years, two studies have investigated diatomic Mb recombination dynamics with ps time resolution. A preliminary study by the Chergui group used 85 ps X-ray pulses to measure XANES spectra of myoglobin following the photolysis of NO at a time delay of 50 ps.[78] Due to the sensitivity of XANES to the local structure of bound ligands via multiple scattering effects, the authors were able to infer that they had captured an intermediately bound state of the NO to the active site at this early time delay. By modeling the XANES with the MXAN software package and fitting the theoretical density of states to their transient XANES, they described this intermediate as having a Fe-N_{NO} bond elongated by about 1Å, slightly longer Fe-N_{His} bond lengths and an intermediate degree of doming of the heme where the Fe atom was placed at 0.16Å out of the heme plane in the direction of the axial histidine as opposed to 0.2Å in deoxy myoglobin.

Recently, our group was able to track the recombination dynamics of CO to both myoglobin in solution and the heme cofactor (Fe protoprophyrin IX) in solution with histidine mimic 1-methyl imidazole. With an energy range covering both the XANES and EXAFS portions of the Fe K-edge,[59] we were able to investigate both electronic changes in the metal center, such as the rearrangement of the d-levels, and minute structural changes in the Fe heme. Within the limit of the 100ps X-ray pulse following photodissociation, a large change in the Fe edge position takes place. Due to the slow recombination rate of CO this change persists for 10s of µs, also indicating that the process of dissociation is complete within the first 100ps. The edge shift is accompanied by the transition from two distinguishable d-level transitions in the XANES to one at a slightly lower energy, a change associated with the transition from low spin d^6 pseudo octahedral to high spin with the loss of a strong field ligand.

Analysis of the EXAFS portion of the XTA spectra of Mb-CO allowed for a detailed structural analysis of the active site heme in addition to the observation of XANES changes following photolysis. Because deoxyMb has been extensively characterized by transient X-ray crystallography[130-133] and steady state EXAFS,[64] a ferric-Mb crystal structure (PDB structure code: 3rj6) was used as the fitting model for for the photolyzed Mb. By fitting to scattering shells calculated for a deoxyMb active site, a penta coordinated, domed structure was confirmed for the photoexcited Mb. This result is consistent with previous time resolved[134, 135] and intermediate trapping crystallographic studies[136] that indicate a deoxy-like structure for the photolyzed Mb. A side by side comparison of the protein bond and free heme (Fe protoporphyrin IX in 1-methyl imidazole), measured in a complimentary study, provides insight into the effects of the protein matrix on ligand binding

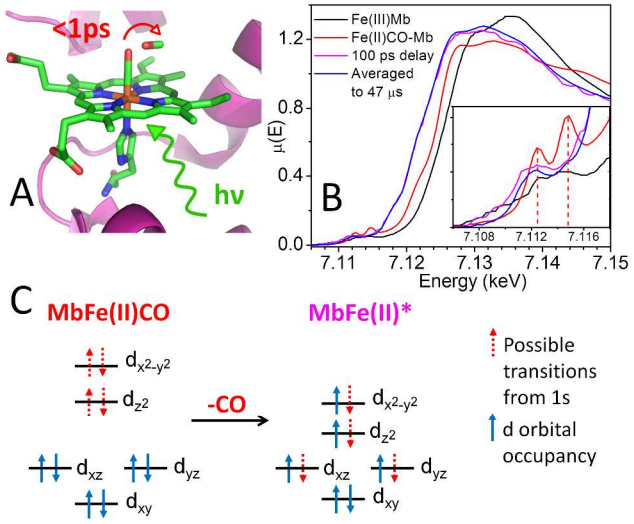

Figure 9. A) the myoglobin heme and surrounding, B) XANES spectra of myoglobin-CO in the ground state and photodissociated state (Reference 59); C) the molecular orbital arrangements in myoglobin-CO and its dissociated product.

by myoglobin. The structure adopted by the deoxy heme following photolysis is very similar to that of myoglobin and both possess a doming distortion of the porphyrin where the Fe sits 0.5Å out of the plane of the porphyrin. It is this out of plane movement of the Fe, or rather the reverse when Hb binds dioxygen, that causes the axial histidine displacement and thus triggers a long range structural reorganization of the protein tertiary structure. That the degree of "doming" in the photoexcited states of both the Fe protoporphyrin and myoglobin are very similar indicates that the protein matrix is capable of maintaining significant communication between itself and the protein heme center while still allowing for full structural relaxation of the heme. This allows motions of the heme following photolysis to initiate long range protein reorganization while simultaneously minimizing the energy of the active site.

Interfacial charge transfer Photo-driven interfacial electron/charge transfer between the transition metal based absorbers and semiconductor nanocrystals on which they are bound has important applications in solar cells, quantum dot devices and photocatalytic hydrogen generation. Both the structural evolution of the adsorbed dye sensitizer and the

rearrangement of the nanocrystal surface associated with the electron density shift during and after the interfacial charge injection are of great interest. Using X-ray transient absorption spectroscopy (XTA), we have measured transient electronic and geometric structures of a ruthenium complex dye sensitizer undergoing interfacial photoinduced charge separation, mimicking the electron injection process in dye sensitized solar cells (DSSCs).[126]

The dye sensitizer used in the sudy was RuN3 ($Ru^{II}(dcbpy)_2(NCS)_2$ in which dcbpy is 4,4'-dicarboxy-2,2'-bipyridine). The laser pump pulse triggered a metal-to-ligand-charge-transfer (MLCT) of RuN3, causing one electron to be injected into the TiO_2 nanoparticle (NP). At a time delay of 50 picoseconds (ps), X-ray probe pulses were used to capture the transient structures of the interfacial system. The approach to data analysis[137, 138] combines quantitative XANES fitting using the multidimensional interpolation approach implemented in the FitIt code and full multiple scattering (FMS) calculations of XAS using FEFF8.2 was used to fit the transient spectra to extract structural parameters for both the ground state and the charge-separated state. Experimentally measured and theoretically calculated XAS signals agree reasonably well. Based on the data analysis, the average Ru-N(NCS) bond length shortens by about 0.06 Å, from 2.05 Å to 1.99 Å upon the conversion from the ground state RuN3/TiO_2 to $RuN3^+/TiO_2^-$, whereas the average Ru-N (dcbpy) bond length only changes within the experimental error from 2.04 Å to 2.05 Å. The different responses in the Ru-N bond lengths in dcbpy and NCS ligands have been directly characterized and rationalized by the interplay between two important factors governing the metal to ligand bonds, the bond order and the steric hindrance. Later on, while seeking cost-efficient photosensitizers to replace the Ru complexes, we also studied the Cu(I) diimine complexes as dye sensitizers on TiO_2 NP surfaces.[139]

So far, the XTA work on interfacial charge transfer mainly has used colloidal solutions of the dye sensitized semiconductor nanoparticles. We are currently developing the grazing-incidence XTA technique. This will open new possibilities to conceptualize and understand details of photoexcited dyes during exciton generation, charge separation and charge transport processes in real-world device configurations.

Femtosecond X-ray Spectroscopy Studies at the X-ray free Electron Laser Sources To address the questions of ultrafast structural dynamics, it is critical to access the time scale on which atomic motions and rearrangements occur. Expanding the capability of X-ray sources into the femotosecond regime, the range into which a single atomic vibrational period will generally fall, is critical to capture chemical processes of interest. The time resolution of transient X-ray spectroscopies at synchrotron sources is generally limited by the temporal width of the X-ray pulse, typically greater than 30ps, making observation of the fastest nuclear rearrangements on excitation difficult. This limitation is due to the nature of the pulse-generating electron bunches, the duration of which in the storage ring cannot decrease beyond this limit and retain significant charge and desirable characteristics. In recent years, several approaches have been developed to access this critical time regime. Specifically these include the development of femtosecond pulse slicing schemes at existing synchrotrons as well as a new generation of X-ray sources in free electron lasers.

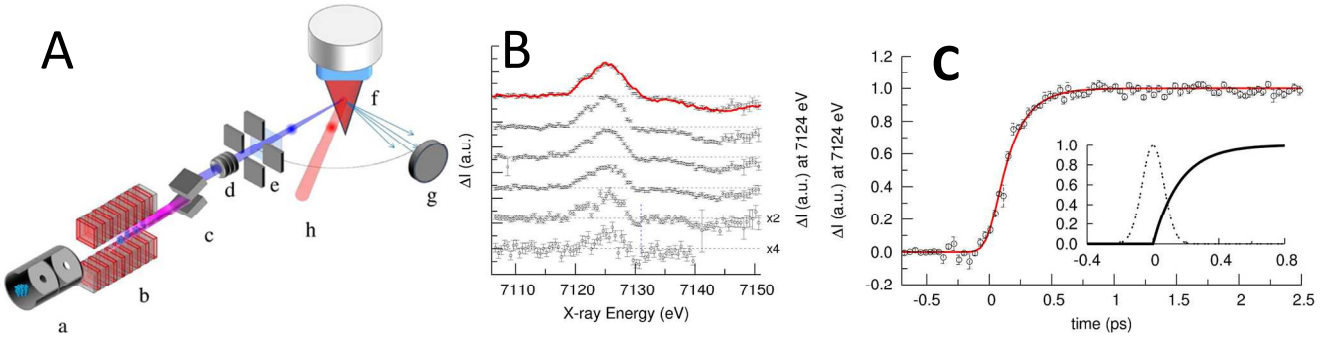

Figure 10. The first femtosecond XANES on Fe(II) tris-bpy complex in solution from Reference 79 . A) The setup at the XPS station of LCLS; B) the difference XANES spectra as a function of the delay time of −170 fs, 0 fs, 190 fs, 370 fs, 550 fs, and 1.25 ps (from bottom to top). The previously measured transient XANES difference signal at 50 ps[11] time delay was scaled and superimposed on the spectrum at the longest time delay (red solid line); the vertical line indicates the isosbestic point for the LS-HS transition; (C) the dynamics of the spin crossover resolved by the femtosecond X-ray pulses at the LCLS shown as the time-dependent amplitude change of the feature at 7125.5 eV (open circles). The resulting fit is shown as a red solid line. The inset of (C) shows the instrument response function (dashed line) function and the exponential rise time (solid line) resulting from the fitting procedure. Copyright of the American Chemical Society.

"Slicing" of conventional synchrotron X-ray pulses into femtosecond pulses involves the energy modulation of a femtosecond slice of the full electron bunch by co-propagation with a femtosecond optical pulse through a wiggler.[72] The major drawback of this method of fs pulse generation is the dramatic reduction in the number of photons per pulse that results from selecting only a small fragment of the pulse duration, and thus signal to noise suffers considerably. Free electron lasers, conversely, offer both very bright and very short pulses, though at a lower repetition rate than most conventional sources. While XFEL X-ray pulses have a duration of only 10s of fs and also boast up to 10^{10}

photons/pulse when a 1 eV bandwidth monochromator is used, the self-amplified spontaneous emission (SASE) processes by which electron bunches are used to generate the X-ray pulses is a highly stochastic process. This "intrinsic instability" results in variation of both the pulse amplitude and energy spectrum from shot to shot, requiring careful normalization. In spite of this, the energy bandwidth of the LCLS beam is sufficient to allow a ~50eV monochromatic scan, sufficient to cover an absorption edge and perform transient XANES. The peak energy of the beam is also tuneable up to about 9.5keV, allowing access to K-edges of most of the first row transition metals.

Spin-crossover dynamics in $[Fe(bipy)_3]^{2+}$ in particular is a good example of coupling between ultrafast electronic dynamics and nuclear rearrangement. $[Fe(bipy)_3]^{2+}$ has a high spin and low spin state which are closely spaced in energy. The high spin state, which possesses a 0.2Å longer Fe-N distance than the LS state, may be accessed through excitation of a metal to ligand charge transfer (MLCT), followed by the eventual relaxation to the high spin quintet.[73] The route of relaxation from the MLCT to the high spin quintet has been somewhat controversial, and was previously thought to proceed through a number of weakly absorbing metal centered singlet and triplet states ($MC\ ^{1,3}T$) with intermediate Fe-N distances. While the HS species is believed to persist with a lifetime of ~600ps based on the recovery of the ground state bleach, the ^{3}MLCT state is depleted in about 120fs.

The HS state has been characterized using XAS at conventional X-ray sources. Analysis of the EXAFS clearly shows a Fe-N bond length shift[111], accompanied by a significant edge shift and rearrangement of pre-edge transitions in the Fe XANES. However, due to the rapid population of the HS state, which appears solely populated at the limiting delay of 50 ps, examination of the nuclear geometry and electronic structure of $[Fe(bipy)_3]^{2+}$ during the relaxation process has so far not been possible with XAS. XAS studies of these complexes have taken advantage of both methods of accessing the femtosecond regime. Using 115 fs pulses from a slicing source at the Swiss Light Source, Bressler and co-workers were able to measure the rise in absorption at an energy corresponding to the so called B feature, a multiple scattering dependent XANES feature associated with the Fe-N distance change seen in the HS state, with a rise time of 150 fs. This kinetic trace was fit to a simple ^{1}MLCT -> ^{3}MLCT -> HS model and the inclusion of MC^3Ts did not produce reasonable lifetimes for those states. An energy scan of the b-feature region at 300 fs proved very similar to that collected at 50 ps previously, confirming the presence of the HS state, though the quality of the XANES data suffered dramatically from the reduced intensity of the fs pulses.

More recently a similar experiment was conducted at LCLS at SLAC National Accelerator Lab using the much brighter X-FEL pulses to collect full XANES scans at several time delays. [79] In this experiment, the instrument response time was limited to about 150fs due to the difference in refractive indices of X-ray and the optical pulses through the liquid jet. Here, some evidence of the MLCT state, which is expected to manifest as a shift of the Fe edge to higher energy because of the decrease in electron density at the Fe, was observed in the form of a dip in the ground state/excited state difference energy spectrum at the HS/LS isosbestic point. Other changes in the energy spectra with time were interpreted as the growing in of the HS state, leaving intact the conclusions of the previous study that the HS state is directly populated from the ^{3}MLCT. A very recent study by Zhang et al. used ultrafast XES to resolve the K_β emission features as a function of time from which they identified the time scale for the spin transition cascade.[140]

Concurrently, the XTA measurements with femtosecond-picosecond time resolution have been carried out at the LCLS in the soft X-ray regime, following the C=O bond breaking on the metal surface, which revealed important structural dynamics information in many catalytic reactions.[141, 142]

Conclusions

The development of ultrafast X-ray spectroscopy in the past decade has enabled this technique to be used in a wide range of chemical systems to take molecular snapshots and movies that allow us to follow chemical reaction coordinates at electron and atomic levels on a time scale comparable to elemental chemical reaction steps, such as bond breakage and formation. In particular, ultrafast X-ray spectroscopy in the hard X-ray regime is a powerful and important tool to extract details of the roles of metal centred d-orbitals in photochemical reactions relevant to solar energy, enzymatic functions and catalysis. These results provide complementary information to those of ultrafast optical spectroscopy, as well as XES and RIXS. The two spectroscpies, when combined, will provide new insight into the nature of transient states, especially those which escaped previous detection. Utilization of ultrafast X-ray spectroscopy combined with other X-ray techniques to study long range structures will enable us to examine electron and nuclear motions simultaneously on nascent excited states as well as electron and nuclear coherence on the femtosecond time scale. As a number of ultrafast X-ray facilities are being built and put into operation, we believe that the frontier of chemical sciences will be advanced to a new level in the decade to come.

Acknowledgements

We thank the support from the U. S. Department of Energy, Office of Science, Office of Basic Energy Sciences, under Contract No. DE-AC02-06CH11357. Use of the Advanced Photon Source at Argonne National Laboratory was supported by the U. S. Department of Energy, Office of Science, Office of Basic Energy Sciences, under Contract No. DE-AC02-06CH11357. The authors would like to thank Drs. K. Attenkofer (now at NSLS-II, Brookhaven National Laboratory), G. Jennings, Q. Kong and Mr. C. Kurtz of the Advanced Photon Source for their contributions in the XTA facility at Beamline 11ID-D, APS. LXC would like to thank her collaborators from both Argonne National Laboratory and Northwestern University, Drs. G. B. Shaw, E. C. Wasinger, J. V. Lockard, M. R. Harpham, A. B. Stickrath, J. Huang, K.

Fransted, D. Hayes, and M. W. Mara for their efforts in experiments mentioned here. Also, many discussions and exchanges with our collaborators, Drs. G. Smolentsev, K. M. Haldrup, Profs. A. Sotadov, S. Della Longa, G. J. Meyer, F. N. Castellano, P. Coppens, J. S. Lindsey, M. P. Hopkins and many others, are appreciated.

Notes and references

[a] Chemical Sciences and Engineering Division, Argonne National Laboratory, 9700 South Cass Avenue, Lemont, Illinois 60439, USA.
[b] Department of Chemistry, Northwestern University, 2145 Sheridan Road, Evanston, Illinois 60208, USA.
[c] X-ray Science Division, Advance Photon Source, Argonne National Laboratory, 9700 South Cass Avenue, Lemont, Illinois 60439, USA.

1. D. E. Sayers, E. A. Stern and F. Lytle, *Phys. Rev. Lett.*, 1971, **27**, 1204-1207.
2. E. A. Stern, D. E. Sayers and F. W. Lytle, *Phys. Rev. B*, 1975, **11**, 4836-4846.
3. F. W. Lytle, D. E. Sayers and E. A. Stern, *Phys. Rev. B*, 1975, **11**, 4825-4835.
4. J. J. Rehr and R. C. Albers, *Reviews of Modern Physics*, 2000, **72**, 621-654.
5. S. I. Zabinsky, J. J. Rehr, A. Ankudinov, R. C. Albers and M. J. Eller, *Physical Review B*, 1995, **52**, 2995-3009.
6. A. L. Ankudinov, B. Ravel, J. J. Rehr and S. D. Conradson, *Physical Review B*, 1998, **58**, 7565-7576.
7. J. J. Rehr, J. M. Deleon, S. I. Zabinsky and R. C. Albers, *Journal of the American Chemical Society*, 1991, **113**, 5135-5140.
8. J. Sa, Y. Kayser, C. J. Milne, D. L. Abreu Fernandes and J. Szlachetko, *Physical chemistry chemical physics : PCCP*, 2014, **16**, 7692-7696.
9. G. Bunker, *Introduction to XAFS: A Practical Guide to X-ray Absorption Fine Structure Spectroscopy*, Cambridge University Press, Cambridge, 2010.
10. D. C. Koningsberg and R. Prins, *X-ray Absorption:Principles, Applications, Techniques of EXAFS, SEXAFS and XANES*, John Wiley & Sons, New York, 1988.
11. M. Rovezzi and P. Glatzel, *Semiconductor Science and Technology*, 2014, **29**.
12. U. Bergmann and P. Glatzel, *Photosynthesis Research*, 2009, **102**, 255-266.
13. J. Kern, R. Alonso-Mori, R. Tran, J. Hattne, R. J. Gildea, N. Echols, C. Glöckner, J. Hellmich, H. Laksmono, R. G. Sierra, B. Lassalle-Kaiser, S. Koroidov, A. Lampe, G. Han, S. Gul, D. DiFiore, D. Milathianaki, A. R. Fry, A. Miahnahri, D. W. Schafer, M. Messerschmidt, M. M. Seibert, J. E. Koglin, D. Sokaras, T.-C. Weng, J. Sellberg, M. J. Latimer, R. W. Grosse-Kunstleve, P. H. Zwart, W. E. White, P. Glatzel, P. D. Adams, M. J. Bogan, G. J. Williams, S. Boutet, J. Messinger, A. Zouni, N. K. Sauter, V. K. Yachandra, U. Bergmann and J. Yano, *Science*, 2013.
14. J. Kern, R. Alonso-Mori, J. Hellmich, R. Tran, J. Hattne, H. Laksmono, C. Glöckner, N. Echols, R. G. Sierra, J. Sellberg, B. Lassalle-Kaiser, R. J. Gildea, P. Glatzel, R. W. Grosse-Kunstleve, M. J. Latimer, T. A. McQueen, D. DiFiore, A. R. Fry, M. Messerschmidt, A. Miahnahri, D. W. Schafer, M. M. Seibert, D. Sokaras, T.-C. Weng, P. H. Zwart, W. E. White, P. D. Adams, M. J. Bogan, S. Boutet, G. J. Williams, J. Messinger, N. K. Sauter, A. Zouni, U. Bergmann, J. Yano and V. K. Yachandra, *PNAS*, 2012.
15. J. Yano, J. Kern, Y. Pushkar, K. Sauer, P. Glatzel, U. Bergmann, J. Messinger, A. Zouni and V. K. Yachandra, *Philosophical Transactions of the Royal Society B-Biological Sciences*, 2008, **363**, 1139-1147.
16. M. Lundberg, T. Kroll, S. DeBeer, U. Bergmann, S. A. Wilson, P. Glatzel, D. Nordlund, B. Hedman, K. O. Hodgson and E. I. Solomon, *Journal of the American Chemical Society*, 2013, **135**, 17121-17134.
17. G. Vanko, A. Bordage, P. Glatzel, E. Gallo, M. Rovezzi, W. Gawelda, A. Galler, C. Bressler, G. Doumy, A. M. March, E. P. Kanter, L. Young, S. H. Southworth, S. E. Canton, J. Uhlig, G. Smolentsev, V. Sundstrom, K. Haldrup, T. B. van Driel, M. M. Nielsen, K. S. Kjaer and H. T. Lemke, *Journal of Electron Spectroscopy and Related Phenomena*, 2013, **188**, 166-171.
18. P. Glatzel, M. Sikora and M. Fernandez-Garcia, *European Physical Journal-Special Topics*, 2009, **169**, 207-214.
19. G. Vanko, P. Glatzel, V.-T. Pham, R. Abela, D. Grolimund, C. N. Borca, S. L. Johnson, C. J. Milne and C. Bressler, *Angewandte Chemie-International Edition*, 2010, **49**, 5910-5912.
20. L. X. Chen, W. J. H. Jäger, G. Jennings, D. J. Gosztola, A. Munkholm and J. P. Hessler, *Science*, 2001, **292**, 262-264.
21. M. Saes, C. Bressler, R. Abela, D. Grolimund, S. L. Johnson, P. A. Heimann and M. Chergui, *Physical Review Letters*, 2003, **90**, 047403/047401-047403/047404.
22. L. X. Chen, *Angew. Chemie, Intl. Ed.*, 2004, **43**, 2886-2905.
23. L. X. Chen, in *Annual Review of Physical Chemistry*, 2005, vol. 56, pp. 221-254.
24. C. Bressler and M. Chergui, *Chemical Reviews (Washington, DC, United States)*, 2004, **104**, 1781-1812.
25. C. Bressler and M. Chergui, *Annual Review of Physical Chemistry*, 2010, **61**, 263-282.
26. L. X. Chen and X. Zhang, *J. Phys. Chem. Lett.*, 2013, **4**, 4000–4013
27. M. A. Brown, A. B. Redondo, I. Jordan, N. Duyckaerts, M.-T. Lee, M. Ammann, F. Nolting, A. Kleibert, T. Huthwelker, J.-P. Maechler, M. Birrer, J. Honegger, R. Wetter, H. J. Woerner and J. A. van Bokhoven, *Review of Scientific Instruments*, 2013, **84**.
28. M. H. Cheng, K. M. Callahan, A. M. Margarella, D. J. Tobias, J. C. Hemminger, H. Bluhm and M. J. Krisch, *Journal of Physical Chemistry C*, 2012, **116**, 4545-4555.
29. A. Y. Klyushin, T. C. R. Rocha, M. Haevecker, A. Knop-Gericke and R. Schloegl, *Physical Chemistry Chemical Physics*, 2014, **16**, 7881-7886.
30. K. Roy and C. S. Gopinath, *Analytical Chemistry*, 2014, **86**, 3683-3687.
31. A. Holmen, A. Broo and B. Albinsson, *Journal of Physical Chemistry*, 1994, **98**, 4998-5009.

32. Y. Jiang, T. Lee and C. G. Rose-Petruck, *Journal of Physical Chemistry A*, 2003, **107**, 7524-7538.
33. T. W. Marin, B. J. Homoelle and K. G. Spears, *Journal of Physical Chemistry A*, 2002, **106**, 1152-1166.
34. A. Vlcek, Jr., *Coordination Chemistry Reviews*, 1998, **177**, 219-256.
35. L. Ujj, C. G. Coates, J. M. Kelly, P. E. Kruger, J. J. McGarvey and G. H. Atkinson, *Journal of Physical Chemistry B*, 2002, **106**, 4854-4862.
36. J. R. Schoonover, G. F. Strouse, K. M. Omberg and R. B. Dyer, *Comments on Inorganic Chemistry*, 1996, **18**, 165-188.
37. K. M. Omberg, G. D. Smith, D. A. Kavaliunas, P. Chen, J. A. Treadway, J. R. Schoonover, R. A. Palmer and T. J. Meyer, *Inorganic Chemistry*, 1999, **38**, 951-956.
38. A. L. Smeigh and J. K. McCusker, 15th International Conference on Ultrafast Phenomena, Pacific Grove, CA, 2006.
39. J. K. McCusker, *Accounts of Chemical Research*, 2003, **36**, 876-887.
40. N. H. Damrauer and J. K. McCusker, *J. Phys. Chem. A*, 1999, **103**, 8440 - 8446.
41. N. H. Damrauer, G. Cerullo, A. Yeh, T. R. Boussie, C. V. Shank and J. K. McCusker, *Science*, 1997, **275**, 54-57.
42. A. Yeh, C. V. Shank and J. K. McCusker, *Science*, 2000, **289**, 935-938.
43. P. F. Barbara, T. J. Meyer and M. A. Ratner, *J. Phys. Chem.*, 1996, **100**, 13148-13168.
44. T. J. Meyer, G. J. Meyer, B. W. Pfennig, J. R. Schoonover, C. J. Timpson, J. F. Wall, C. Kobusch, X. H. Chen, B. M. Peek, C. G. Wall, W. Ou, B. W. Erickson and C. A. Bignozzi, *Inorg. Chem.*, 1994, **33**, 3952-3964.
45. H. Buersing, S. Kundu and P. Voehringer, *Journal of Physical Chemistry B*, 2003, **107**, 2404-2414.
46. R. Argazzi, C. A. Bignozzi, M. Yang, G. M. Hasselmann and G. J. Meyer, *Nano Letters*, 2002, **2**, 625-628.
47. Y. Jiang, W. Li, G. Cao, T. Lee, G. Ketwaroo and C. G. Rose-Petruck, *Proceedings of SPIE-The International Society for Optical Engineering*, 2001, **4504**, 42-48.
48. H. Bursing, D. Ouw, S. Kundu and P. Vohringer, *Physical Chemistry Chemical Physics*, 2001, **3**, 2378-2387.
49. H. Shirota and E. W. Castner, *Journal of Chemical Physics*, 2000, **112**, 2367-2376.
50. L. X. Chen, X. Zhang, E. C. Wasinger, J. V. Lockard, A. B. Stickrath, M. W. Mara, K. Attenkofer, G. Jennings, G. Smolentsev and A. Soldatov, *Chemical Science*, 2010, **1**.
51. L. X. Chen, X. Zhang, E. C. Wasinger, K. Attenkofer, G. Jennings, A. Z. Muresan and J. S. Lindsey, *J. Am. Chem. Soc.*, 2007, **129**, 9616-9618.
52. N. Huse, T. K. Kim, L. Jamula, J. K. McCusker, F. M. F. de Groot and R. W. Schoenlein, *Journal of the American Chemical Society*, 2010, **132**, 6809-6816.
53. A. Cannizzo, C. J. Milne, C. Consani, W. Gawelda, C. Bressler, F. van Mourik and M. Chergui, *Coordination Chemistry Reviews*, 2010, **254**, 2677-2686.
54. N. Huse, H. Cho, K. Hong, L. Jamula, F. M. F. de Groot, T. K. Kim, J. K. McCusker and R. W. Schoenlein, *Journal of Physical Chemistry Letters*, 2011, **2**, 880-884.
55. S. Nozawa, T. Sato, M. Chollet, K. Ichiyanagi, A. Tomita, H. Fujii, S. Adachi and S. Koshihara, *Journal of the American Chemical Society*, 2010, **132**, 61-+.
56. C. Sousa, C. de Graaf, A. Rudavskyi, R. Broer, J. Tatchen, M. Etinski and C. M. Marian, *Chemistry-a European Journal*, 2013, **19**, 17541-17551.
57. M. W. Mara, M. Shelby, A. Stickrath, M. Harpham, J. Huang, X. Zhang, B. M. Hoffman and L. X. Chen, *Journal of Physical Chemistry B*, 2013, **117**, 14089-14098.
58. W. Zeng, Y. Sun, A. Benabbas and P. M. Champion, *Journal of Physical Chemistry B*, 2013, **117**, 4042-4049.
59. A. B. Stickrath, M. W. Mara, J. V. Lockard, M. R. Harpham, X. Zhang, K. Attenkofer and L. X. Chen, *J. Phys. Chem. B.*, 2013, **ASAP DOI 10.1021/jp3086705**.
60. M. R. Harpham, A. B. Stickrath, X. Zhang, J. Huang, M. W. Mara, L. X. Chen and D.-J. Liu, *J. Phys. Chem. A, Articles ASAP*, 2013, **DOI: 10.1021/jp312663q**.
61. J. Chen, H. Zhang, I. V. Tomov, X. L. Ding and P. M. Rentzepis, *Chemical Physics Letters*, 2007, **437**, 50-55.
62. J. J. Regan, B. E. Ramirez, J. R. Winkler, H. B. Gray and B. G. Malmstrom, *Journal of Bioenergetics and Biomembranes*, 1998, **30**, 35-39.
63. H. S. Eom, S. C. Jeoung, D. Kim, J.-H. Ha and Y.-R. Kim, *Journal of Physical Chemistry A*, 1997, **101**, 3661-3669.
64. S. Della Longa, I. Ascone, A. Fontaine, A. Congiu Castellano and A. Bianconi, *Eur. Biophys. J.*, 1994, **23**, 361-368.
65. P. M. Rentzepis and B. Van Wonterghem, *Chem. Energ. Mater.*, 1991, 55-75.
66. K. B. Eisenthal, M. K. Crawford, C. Dupuy, W. Hetherington, G. Korenowski, M. J. McAuliffe and Y. Wang, *Springer Series in Chemical Physics*, 1980, **14**, 220-226.
67. A. Cavalleri, H. H. W. Chong, S. Fourmaux, T. E. Glover, P. A. Heimann, J. C. Kieffer, B. S. Mun, H. A. Padmore and R. W. Schoenlein, *Physical Review B*, 2004, **69**.
68. M. Faubel, K. R. Siefermann, Y. Liu and B. Abel, *Accounts of Chemical Research*, 2012, **45**, 120-130.
69. S. Fourmaux, L. Lecherbourg, M. Harmand, M. Servol and J. C. Kieffer, *Review of Scientific Instruments*, 2007, **78**.
70. N. Huse, H. Wen, D. Nordlund, E. Szilagyi, D. Daranciang, T. A. Miller, A. Nilsson, R. W. Schoenlein and A. M. Lindenberg, *Physical Chemistry Chemical Physics*, 2009, **11**, 3951-3957.
71. K. A. Lomachenko, C. Garino, E. Gallo, D. Gianolio, R. Gobetto, P. Glatzel, N. Smolentsev, G. Smolentsev, A. V. Soldatov, C. Lamberti and L. Salassa, *Physical Chemistry Chemical Physics*, 2013, **15**, 16152-16159.
72. R. W. Schoenlein, S. Chattopadhyay, H. H. W. Chong, T. E. Glover, P. A. Heimann, C. V. Shank, A. A. Zholents and M. S. Zolotorev, *Science*, 2000, **287**, 2237-2240.
73. C. Bressler, C. Milne, V. T. Pham, A. ElNahhas, R. M. v. d. Veen, W. Gawelda, S. Johnson, P. Beaud, D. Grolimund, M. Kaiser, C. N. Borca, G. Ingold, R. Abela and M. Chergui, *Science*, 2009, **323**, 489-492.
74. M. Beye, P. Wernet, C. Schussler-Langeheine and A. Fohlisch, *Journal of Electron Spectroscopy and Related Phenomena*, 2013, **188**, 172-182.

75. A. Nilsson, T. Tokushima, Y. Horikawa, Y. Harada, M. P. Ljungberg, S. Shin and L. G. M. Pettersson, *Journal of Electron Spectroscopy and Related Phenomena*, 2013, **188**, 84-100.
76. P. Glatzel and U. Bergmann, *Coordination Chemistry Reviews*, 2005, **249**, 65-95.
77. A. M. March, A. B. Stickrath, G. Doumy, E. P. Kanter, B. Kr¨assig, S. H. Southworth, K. Attenkofer, C. A. Kurtz, L. X. Chen and L. Young, *Rev. Sci. Inst.*, 2011, **82**, 073110.
78. F. A. Lima, C. J. Milne, D. C. V. Amarasinghe, M. H. Rittmann-Frank, R. M. van der Veen, M. Reinhard, V.-T. Pham, S. Karlsson, S. L. Johnson, D. Grolimund, C. Borca, T. Huthwelker, M. Janousch, F. van Mourik, R. Abela and M. Chergui, *Rev. Sci. Instrum.*, 2011, **82**, 063111-063126.
79. H. T. Lemke, C. Bressler, L. X. Chen, D. M. Fritz, K. J. Gaffney, A. Galler, W. Gawelda, K. Haldrup, R. W. Hartsock, H. Ihee, J. Kim, K. H. Kim, J. H. Lee, M. M. Nielsen, A. B. Stickrath, W. Zhang, D. Zhu and M. Cammarata, *Journal of Physical Chemistry A*, 2013, **117**, 735 - 740.
80. G. Schiwietz, M. Beye, K. Czerski, A. Fohlisch, R. Konnecke, M. Roth, J. Schlappa, F. Staufenbiel, E. Suljoti, I. Kuusik and P. L. Grande, *Nuclear Instruments & Methods in Physics Research Section B-Beam Interactions with Materials and Atoms*, 2013, **317**, 48-55.
81. M. Tromp, A. J. Dent, J. Headspith, T. L. Easun, X. Z. Sun, M. W. George, O. Mathon, G. Smolentsev, M. L. Hamilton and J. Evans, *Journal of Physical Chemistry B*, 2013, **117**, 7381-7387.
82. A. El Nahhas, R. M. van der Veen, T. J. Penfold, V. T. Pham, F. A. Lima, R. Abela, A. M. Blanco-Rodriguez, S. Zalis, A. Vlcek, I. Tavernelli, U. Rothlisberger, C. J. Milne and M. Chergui, *Journal of Physical Chemistry A*, 2013, **117**, 361-369.
83. J. Vura-Weis, C. M. Jiang and S. R. Leone, *Abstracts of Papers of the American Chemical Society*, 2012, **244**.
84. T. Sato, S. Nozawa, A. Tomita, M. Hoshino, S. Y. Koshihara, H. Fujii and S. Adachi, *Journal of Physical Chemistry C*, 2012, **116**, 14232-14236.
85. B. E. Van Kuiken, N. Huse, H. Cho, M. L. Strader, M. S. Lynch, R. W. Schoenlein and M. Khalil, *Journal of Physical Chemistry Letters*, 2012, **3**, 1695-1700.
86. J. V. Lockard, S. Kabehie, G. Smolentsev, A. Soldatov, J. I. Zink and L. X. Chen, *J. Phys. Chem. B*, 2010, **114**, 14521–14527.
87. J. Huang, O. Buyukcakir, M. W. Mara, A. Coskun, N. M. Dimitrijevic, G. Barin, O. Kokhan, A. B. Stickrath, R. Ruppert, D. M. Tiede, J. F. Stoddart, J. P. Sauvage and L. X. Chen, *Angewandte Chemie-International Edition*, 2012, **51**, 12711-12715.
88. J. Chang, A. J. Fedro and M. van Veenendaal, *Chemical Physics*, 2012, **407**, 65-70.
89. R. M. van der Veen, J. J. Kas, C. J. Milne, V. T. Pham, A. El Nahhas, F. A. Lima, D. A. Vithanage, J. J. Rehr, R. Abela and M. Chergui, *Physical Chemistry Chemical Physics*, 2010, **12**, 5551-5561.
90. S. E. Canton, X. Y. Zhang, L. M. L. Daku, A. L. Smeigh, J. X. Zhang, Y. Z. Liu, C. J. Wallentin, K. Attenkofer, G. Jennings, C. A. Kurtz, D. Gosztola, K. Warnmark, A. Hauser and V. Sundstrom, *Journal of Physical Chemistry C*, 2014, **118**, 4536-4545.
91. J. V. Lockard, S. Kabehie, J. I. Zink, G. Smolentsev, A. Soldatov and L. X. Chen, *Journal of Physical Chemistry B*, 2010, **114**, 14521-14527.
92. K. Haldrup, G. Vanko, W. Gawelda, A. Galler, G. Doumy, A. M. March, E. P. Kanter, A. Bordage, A. Dohn, T. B. van Driel, K. S. Kjaer, H. T. Lemke, S. E. Canton, J. Uhlig, V. Sundstrom, L. Young, S. H. Southworth, M. M. Nielsen and C. Bressler, *Journal of Physical Chemistry A*, 2012, **116**, 9878-9887.
93. B. E. Van Kuiken and M. Khalil, *Journal of Physical Chemistry A*, 2011, **115**, 10749-10761.
94. T. Hasobe, H. Sakai, K. Mase, K. Ohkubo and S. Fukuzumi, *Journal of Physical Chemistry C*, 2013, **117**, 4441-4449.
95. V. Balzani and Editor, *Electron Transfer in Chemistry, Volume 1*, Wiley-VCH, Weinheim, 2001.
96. M. T. Vagnini, M. W. Mara, M. R. Harpham, J. Huang, M. L. Shelby, L. X. Chen and M. R. Wasielewski, *Chemical Science*, 2013, **4**, 3863-3873.
97. S. E. Canton, X. Y. Zhang, J. X. Zhang, T. B. van Driel, K. S. Kjaer, K. Haldrup, P. Chabera, T. Harlang, K. Suarez-Alcantara, Y. Z. Liu, J. Perez, A. Bordage, M. Papai, G. Vanko, G. Jennings, C. A. Kurtz, M. Rovezzi, P. Glatzel, G. Smolentsev, J. Uhlig, A. O. Dohn, M. Christensen, A. Galler, W. Gawelda, C. Bressler, H. T. Lemke, K. B. Moller, M. M. Nielsen, R. Lomoth, K. Warnmark and V. Sundstrom, *Journal of Physical Chemistry Letters*, 2013, **4**, 1972-1976.
98. S. Ardo and G. J. Meyer, *Chem. Soc. Rev.*, 2009, **38**, 115-164.
99. N. Armaroli, *Chem. Soc. Rev.*, 2001, **30**, 113-124.
100. V. W. W. Yam, *Accounts of Chemical Research*, 2002, **35**, 555-563.
101. R. Schweitzer-Stenner, C. Lemke, R. Haddad, Y. Qiu, J. A. Shelnutt, J. M. E. Quirke and W. Dreybrodt, *Journal of Physical Chemistry A*, 2001, **105**, 6680-6694.
102. C. J. Medforth, M. O. Senge, K. M. Smith, L. D. Sparks and J. A. Shelnutt, in *J. Am. Chem. Soc.*, 1992, vol. 114, pp. 9859-9869.
103. R. G. Alden, B. A. Crawford, R. Doolen, M. R. Ondrias and J. A. Shelnutt, *J. Am. Chem. Soc.*, 1989, **111**, 2070-2072.
104. D. Kim, C. Kirmaier and D. Holten, *Chem. Phys.*, 1983, **75**, 305-322.
105. P. Gutlich, Y. Garcia and T. Woike, *Coordination Chemistry Reviews*, 2001, **219**, 839-879.
106. P. Gutlich, A. Hauser and H. Spiering, *Angewandte Chemie-International Edition in English*, 1994, **33**, 2024-2054.
107. A. Hauser, *Journal of Chemical Physics*, 1991, **94**, 2741-2748.
108. Khalil M, Marcus MA, Smeigh AL, McCusker JK, Chong HHW and S. RW, *Journal of Physical Chemistry A*, 2006, **110**, 38-44.
109. Khalil M, Marcus MA, Smeigh AL, McCusker JK, Chong HHW and S. RW, *J. Phys. Chem. A*, 2006, **110**, 38-44.
110. W. Gawelda, A. Cannizzo, V.-T. Pham, F. van Mourik, C. Bressler and M. Chergui, *Journal of the American Chemical Society*, 2007, **129**, 8199-8206.

111. W. Gawelda, V.-T. Pham, M. Benfatto, Y. Zaushitsyn, M. Kaiser, D. Grolimund, S. L. Johnson, R. Abela, A. Hauser, C. Bressler and M. Chergui, *Physical Review Letters*, 2007, **98**.
112. C. Bressler, C. Milne, V. T. Pham, A. ElNahhas, R. M. van der Veen, W. Gawelda, S. Johnson, P. Beaud, D. Grolimund, M. Kaiser, C. N. Borca, G. Ingold, R. Abela and M. Chergui, *Science*, 2009, **323**, 489-492.
113. M. R. Harpham, S. C. Nguyen, Z. Hou, J. C. Grossman, C. B. Harris, M. W. Mara, A. B. Stickrath, Y. Kanai, A. M. Kolpak, D. Lee, D.-J. Liu, J. P. Lomont, K. Moth-Poulsen, N. Vinokurov, L. X. Chen and K. P. C. Vollhardt, *Angewandte Chemie-International Edition*, 2012, **51**, 7692-7696.
114. W. Gawelda, V. T. Pham, R. M. van der Veen, D. Grolimund, R. Abela, M. Chergui and C. Bressler, *Journal of Chemical Physics*, 2009, **130**.
115. W. Gawelda, M. Johnson, F. M. F. de Groot, R. Abela, C. Bressler and M. Chergui, *Journal of the American Chemical Society*, 2006, **128**, 5001-5009.
116. J. V. Lockard, A. A. Rachford, G. Smolentsev, A. B. Stickrath, X. Wang, X. Zhang, K. Atenkoffer, G. Jennings, A. Soldatov, A. L. Rheingold, F. N. Castellano and L. X. Chen, *J. Phys. Chem. A.*, 2010, **114**, 12780-12787
117. R. M. van der Veen, C. J. Milne, A. El Nahhas, F. A. Lima, V. T. Pham, J. Best, J. A. Weinstein, C. N. Borca, R. Abela, C. Bressler and M. Chergui, *Angewandte Chemie-International Edition*, 2009, **48**, 2711-2714.
118. L. X. Chen and X. Zhang, *J. Phys. Chem. Lett.* , 2013, **4**, 4000–4013.
119. L. X. Chen, X. Zhang, J. V. Lockard, A. B. Stickrath, K. Attenkofer, G. Jennings and D.-J. Liu, *Acta Crystallographica Section A Foundations of Crystallography*, 2010, **66**, 240-251.
120. E. Borfecchia, C. Garino, L. Salassa, T. Ruiu, D. Gianolio, X. Y. Zhang, K. Attenkofer, L. X. Chen, R. Gobetto, P. J. Sadler and C. Lamberti, *Dalton Transactions*, 2013, **42**, 6564-6571.
121. B. E. Van Kuiken, M. Valiev, S. L. Daifuku, C. Bannan, M. L. Strader, H. N. Cho, N. Huse, R. W. Schoenlein, N. Govind and M. Khalil, *Journal of Physical Chemistry A*, 2013, **117**, 4444-4454.
122. M. R. Harpham, A. B. Stickrath, X. Y. Zhang, J. Huang, M. W. Mara, L. X. Chen and D. J. Liu, *Journal of Physical Chemistry A*, 2013, **117**, 9807-9813.
123. M. T. Vagnini, M. W. Mara, M. R. Harpham, J. Huang, M. L. Shelby, L. X. Chen and M. R. Wasielewski, *Chemical Science*, 2013, **DOI: 10.1039/c3sc51511g**.
124. H. Wang, G. Peng and S. P. Cramer, *Journal of Electron Spectroscopy and Related Phenomena*, 2005, **143**, 1-7.
125. M. W. Mara, M. Shelby, A. Stickrath, M. Harpham, J. E. Huang, X. Y. Zhang, B. M. Hoffman and L. X. Chen, *Journal of Physical Chemistry B*, 2013, **117**, 14089-14098.
126. X. Zhang, G. Smolentsev, J. Guo, K. Attenkofer, C. Kurtz, G. Jennings, J. V. Lockard, A. B. Stickrath and L. X. Chen, *The Journal of Physical Chemistry Letters*, 2011, **2**, 628-632.
127. H. Dau and M. Haumann, *Photosynthesis Research*, 2007, **92**, 327-343.
128. M. Haumann, A. Grundmeier, I. Zaharieva and H. Dau, *Proceedings of the National Academy of Sciences of the United States of America*, 2008, **105**, 17384-17389.
129. D. M. Mills, A. Lewis, A. Harootunian, J. Huang and B. Smith, *Science*, 1984, **223**, 811-813.
130. F. Schotte, J. Soman, J. S. Olson, M. Wulff and P. A. Anfinrud, *Journal of Structural Biology*, 2004, **147**, 235-246.
131. F. Schotte, M. Lim, T. A. Jackson, A. V. Smirnov, J. Soman, J. S. Olson, G. N. Phillips, Jr., M. Wulff and P. A. Anfinrud, *Science*, 2003, **300**, 1944-1947.
132. V. Srajer, Z. Ren, T.-Y. Teng, M. Schmidt, T. Ursby, D. Bourgeois, C. Pradervand, W. Schildkamp, M. Wulff and K. Moffat, *Biochemistry*, 2001, **40**, 13802-13815.
133. V. Srajer, T.-y. Teng, T. Ursby, C. Pradervand, Z. Ren, S.-i. Adachi, W. Schildkamp, D. Bourgeois, M. Wulff and K. Moffat, *Science (Washington, D. C.)*, 1996, **274**, 1726-1729.
134. R. Aranda, E. J. Levin, F. Schotte, P. A. Anfinrud and G. N. Phillips, *Acta Crystallographica Section D Biological Crystallography*, 2006, **62**, 776-783.
135. J. Vojtěchovský, K. Chu, J. Berendzen, R. M. Sweet and I. Schlichting, *Biophysical Journal*, 1999, **77**, 2153-2174.
136. M. Salmeron and R. Schlogl, *Surface Science Reports*, 2008, **63**, 169-199.
137. G. Smolentsev and A. V. Soldatov, *Computational Materials Science*, 2007, **39**, 569-574.
138. G. Smolentsev and A. Soldatov, *Journal of Synchrotron Radiation*, 2006, **13**, 19-29.
139. J. Huang, O. Buyukcakir, M. W. Mara, A. Coskun, N. M. Dimitrijevic, G. Barin, O. Kokhan, A. B. Stickrath, R. Ruppert, D. M. Tiede, J. F. Stoddart, J.-P. Sauvage and L. X. Chen, *Angewandte Chemie International Edition*, 2012, **51**, 12711-12715.
140. W. Zhang, R. Alonso-Mori, U. Bergmann, C. Bressler, M. Chollet, A. Galler, W. Gawelda, R. G. Hadt, R. W. Hartsock, T. Kroll, K. S. Kjaer, K. Kubicek, H. T. Lemke, H. W. Liang, D. A. Meyer, M. M. Nielsen, C. Purser, J. S. Robinson, E. I. Solomon, Z. Sun, D. Sokaras, T. B. van Driel, G. Vanko, T.-C. Weng, D. Zhu and K. J. Gaffney, *Nature*, 2014, **509**, 345-+.
141. M. Beye, T. Anniyev, R. Coffee, M. Dell'Angela, A. Foehlisch, J. Gladh, T. Katayama, S. Kaya, O. Krupin, A. Mogelhoj, A. Nilsson, D. Nordlund, J. K. Norskov, H. Oberg, H. Ogasawara, L. G. M. Pettersson, W. F. Schlotter, J. A. Sellberg, F. Sorgenfrei, J. J. Turner, M. Wolf, W. Wurth and H. Ostrom, *Physical Review Letters*, 2013, **110**.
142. M. Dell'Angela, T. Anniyev, M. Beye, R. Coffee, A. Foehlisch, J. Gladh, T. Katayama, S. Kaya, O. Krupin, J. LaRue, A. Mogelhoj, D. Nordlund, J. K. Norskov, H. Oberg, H. Ogasawara, H. Ostrom, L. G. M. Pettersson, W. F. Schlotter, J. A. Sellberg, F. Sorgenfrei, J. J. Turner, M. Wolf, W. Wurth and A. Nilsson, *Science*, 2013, **339**, 1302-1305.

